ACS Catalysis

Letter

pubs.acs.org/acscatalysis

Self-Supported FeP Nanorod Arrays: A Cost-Effective 3D Hydrogen Evolution Cathode with High Catalytic Activity

Yanhui Liang,[†] Qian Liu,[†] Abdullah M. Asiri,[§,∥] Xuping Sun,*[,†,§,∥] and Yonglan Luo*[,†]

[†]Chemical Synthesis and Pollution Control Key Laboratory of Sichuan Province, College of Chemistry and Chemical Engineering, China West Normal University, Nanchong 637002, Sichuan, China

[§]Chemistry Department, Faculty of Science, King Abdulaziz University, Jeddah 21589, Saudi Arabia

[∥]Center of Excellence for Advanced Materials Research, King Abdulaziz University, Jeddah 21589, Saudi Arabia

Supporting Information

ABSTRACT: Developing non-noble-metal hydrogen evolution reaction electrocatalysts with high activity is critical for future renewable energy systems. The direct growth of active phases on current collectors not only eliminates using polymer binder but also offers time-saving preparation of electrode. In this Letter, we develop self-supported FeP nanorod arrays on carbon cloth (FeP NAs/CC) via low-temperature phosphidation of its Fe_2O_3 NAs/CC. As a novel 3D hydrogen evolution cathode in acidic media, the FeP NAs/CC exhibits high catalytic activity and only needs an overpotential of 58 mV to afford current density of 10 mA/cm^2. This electrode also works efficiently in both neutral and alkaline solutions.

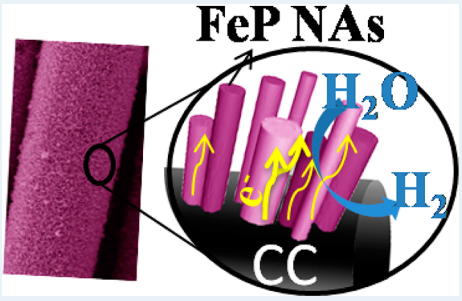

KEYWORDS: *FeP, nanorod arrays, binder-free, 3D hydrogen evolution cathode, electrocatalysis, water splitting*

The rapid depletion of fossil fuels and increased environmental concerns has caused an urgent demand for searching clean and sustainable alternative energy sources.[1,2] Hydrogen is an abundant and renewable clean chemical fuel to replace fossil fuels in the future.[3−5] Splitting water offers one simple way to produce hydrogen but needs an efficient electrocatalyst for the hydrogen evolution reaction (HER) to afford high current at low overpotential.[6] The best HER catalysts currently consist of Pt or Pt-based materials with negligible overpotentials and excellent kinetics for driving the HER,[7,8] but such catalysts suffer from high cost. Water electrolysis based on proton exchange membrane (PEM) technology operates under strongly acidic conditions.[9] Although abundant nickel-based alloys have been widely used commercially as HER catalysts,[10,11] they cannot operate in strongly acidic media. These limitations have motivated great research effort to develop acid-stable non-noble-metal HER catalysts, and significant recent progress has been made toward this direction in past years. Among such catalysts, Mo-based compounds have received intensive attention with great success, including MoS_2,[12−15] MoSe,[16] MoB,[17] Mo_2C,[17−19] $NiMoN_x$,[20] $Co_{0.6}Mo_{1.4}N_2$,[21] among others.

Transition metal phosphides (TMPs) have good electrical conductivity and have been widely used as catalysts for hydrodesulfurization (HDS) and hydrodenitrogenation (HDN) as well as anode materials for Li-ion batteries (LIBs).[22,23] Recent studies have shown that TMPs are active toward hydrogen evolution in acidic electrolytes, including Ni_2P,[24−26] CoP,[27−39] Cu_3P,[30] MoP,[31−33] WP,[34] and FeP nanosheets[35]. This FeP catalyst, however, needs a large overpotential (η) of ∼240 mV to afford a current density of 10 mA/cm^2 and requires using several organic solvents and multiple tedious time-consuming steps for preparation.[35]

Electrochemical tests require effective immobilization of electrocatalysts on conductive substrates as current collectors with the use of a polymer binder as a film-forming agent. The polymer binder, however, increases the series resistance[36] and may block active sites and inhibit diffusion, leading to reduced catalytic activity.[37] Such issues can be solved by directly growing the active phases on conductive substrates as the current collectors.[26,29,30] Iron is the cheapest and one of the most abundant of all transition metals, whereas carbon is the most abundant element on earth. The combination of Fe-based active phases and carbon support will offer us the most cost-effective HER catalysts. In this Letter, we report the growth of FeP nanorod arrays on carbon cloth (FeP NAs/CC) via low-temperature phosphidation of their Fe_2O_3 NAs/CC precursor. When used as a binder-free 3D hydrogen evolution cathode in acidic media, the FeP NAs/CC exhibits high catalytic activity and good durability with a small onset overpotential of 20 mV, a low Tafel slope of 45 mV/dec, a large exchange current density of 0.50 mA/cm^2, and nearly 100% Faradaic efficiency. It needs overpotentials of 58 mV to achieve current density of 10 mA/cm^2. This electrode is also able to perform efficiently in both neutral and alkaline electrolytes.

Received: July 31, 2014
Revised: October 15, 2014
Published: October 15, 2014

   dx.doi.org/10.1021/cs501106g | ACS Catal. 2014, 4, 4065−4069

Figure S1 shows the X-ray diffraction (XRD) patterns of Fe_2O_3 precursor and FeP scratched from CC. The precursor shows peaks at 33.2°, 35.7°, 40.9°,49.5°, 54.1°, 62.6°, and 64.1° indexed to (104), (110), (113), (024), (116), (214), and (300) planes of Fe_2O_3, respectively (JCPDS No. 84-0306). The phosphided product shows diffraction peaks at 32.8°, 37.2°, 46.4°, 47.0°, 48.4°, 50.5°, 56.1°, and 59.6° indexed to (011), (111), (112), (202), (211), (103), (212), and (020) planes of FeP, respectively (JCPDS No. 78-1443). The energy dispersive X-ray (EDX) spectrum shows nearly 1:1 atomic ratio of Fe/P (Figure S2).The exact Fe/P atomic ratio for this catalyst was further determined to be 1:1.09 by inductively coupled plasma mass spectrometry (ICP-MS) analysis. The low-magnification scanning electron microscopy (SEM) image shows that CC was full covered with Fe_2O_3 structures (Figure 1a). The high-magnification SEM image (Figure 1a inset) further reveals that these Fe_2O_3 structures are aligned nanorod arrays. After phosphidation, the morphology of such nanorod arrays was well maintained (Figure 1b). The transmission electron microscopy (TEM) image (Figure 1c) also confirms the nanorod nature of the phosphided product. The high-resolution TEM (HRTEM) image (Figure 1d) shows well-resolved lattice fringes with an interplanar distance of 0.27 nm corresponding to the (011) plane of FeP. The selected area electron diffraction (SAED) pattern (Figure 1e) shows discrete spots indexed to the (011), (002), (201), and (211) planes of orthorhombic FeP structure. The scanning TEM (STEM) image and the corresponding EDX elemental mapping images of C, P, and Fe for FeP NAs/CC reveal that both P and Fe elements are uniformly distributed throughout FeP NAs/CC (Figure 1f). All these results strongly verify the successful chemical conversion of Fe_2O_3 NAs/CC into FeP NAs/CC via the low-temperature phosphidation. The same preparation without using CC, however, only leads to Fe_2O_3 microparticles (Fe_2O_3 MPs) consisting of nanorods and the following phosphidation produces FeP microparticles (FeP MPs), as shown in Figure S3 and S4.

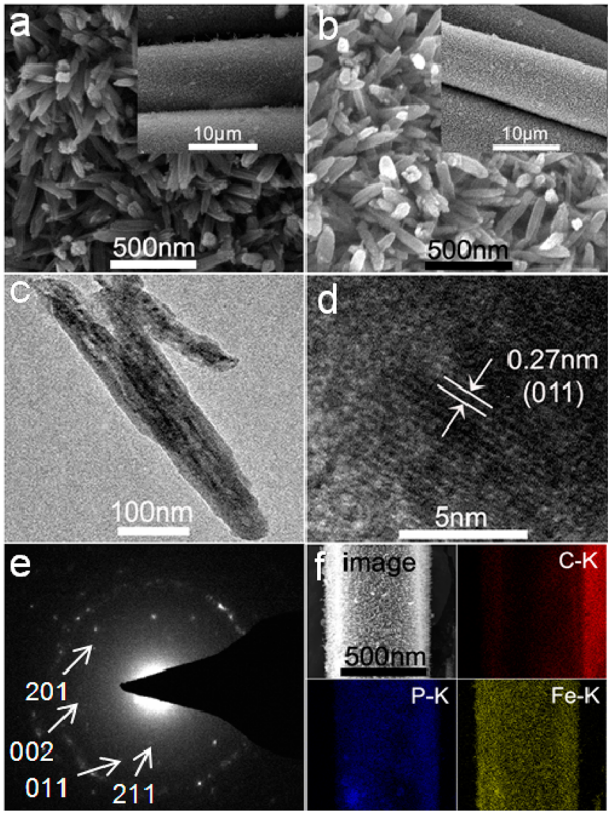

Figure 1. SEM images of (a) Fe_2O_3 NAs/CC and (b) FeP NAs/CC. (c) TEM and (d) HRTEM images of FeP nanorods. (e) SAED pattern recorded from the FeP nanorod. (f) STEM image and EDX elemental mapping of C, P, and Fe for the FeP NAs/CC.

The activity of FeP NAs/CC (FeP loading: ~1.5 mg/cm^2) was studied in a typical three-electrode setup with 0.5 M H_2SO_4 electrolyte. Blank CC and commercial Pt/C (20 wt % Pt/XC-72) were also tested for comparison. A resistance test was made, and an *iR* correction was applied to all initial data for further analysis. Figure 2a shows the polarization curves. The Pt/C catalyst exhibits expected HER activity with a near zero overpotential while blank CC shows very poor HER activity. The FeP NAs/CC is highly active toward the HER with an onset overpotential of 20 mV and only needs overpotential of 58 mV to afford current density of 10 mA/cm^2. This overpotential compares favorably to the behaviors of FeP nanosheets[35] and other reported non-noble-metal HER catalysts in acidic solutions (Table S1). Compared to the recently reported FeP array on a Ti plate, FeP NAs/CC shows comparable[38] or even superior[39] catalytic activity and the

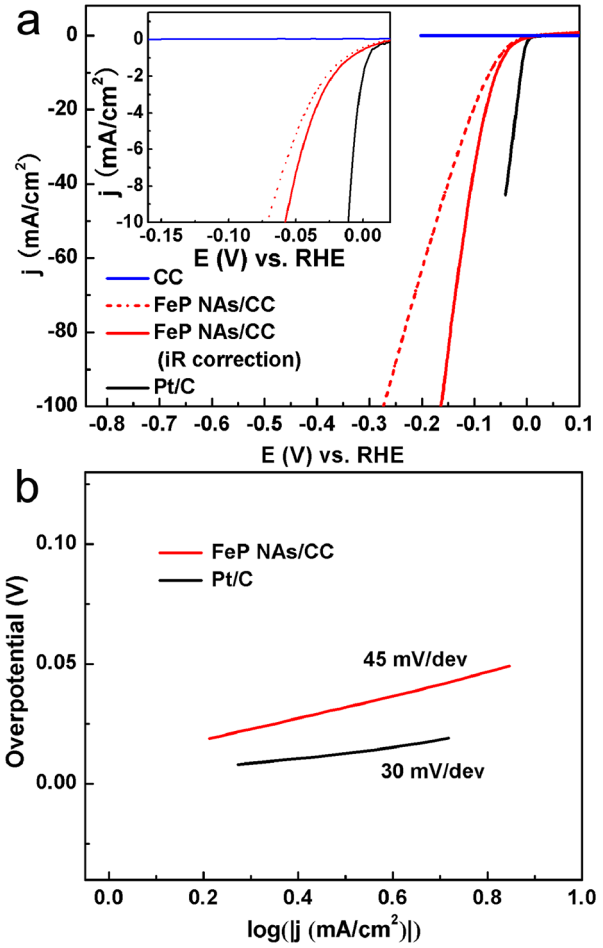

Figure 2. (a) Polarization curves for Pt/C, FeP NAs/CC, and CC in 0.5 M H_2SO_4 solution with a scan rate of 2 mV/s. (b) Tafel plots for Pt/C and FeP NAs/CC.

dx.doi.org/10.1021/cs501106g | *ACS Catal.* 2014, 4, 4065−4069

excellent flexibilility of CC also facilitates easier integration of this electrode into devices for applications.

Figure 2b shows the Tafel plots for Pt/C and FeP NAs/CC. The curves in the low current density region show Tafel slopes of 30 and 45 mV/dec for Pt/C and FeP NAs/CC, respectively. This Tafel slope for FeP NAs/CC reveals the HER may proceed via a Volmer–Heyrovsky mechanism.[40,41] The exchange current density (j_0) of FeP NAs/CC was calculated to be 0.50 mA/cm^2 by applying the extrapolation method to the Tafel plot, much higher than those of FeP MPs/CC (0.03 mA/cm^2) (Figure S5) and other Pt-free HER catalysts listed in Table S1.

FeP MPs coated on CC (FeP MPs/CC) using nafion is also electroactive toward the HER (FeP loading: 1.5 mg/cm^2, Figure S6). Compared to FeP NAs/CC, this electrode shows much larger onset overpotential of 130 mV and affords current density of 5 mA/cm^2 at η = 163 mV, implying much superior catalytic activity of FeP NAs/CC. Electrochemical impedance spectroscopy analysis shows FeP NAs/CC has much lower impedance and thus markedly faster HER kinetics than FeP MPs/CC (Figure S7). The capacitances of the double layer at the solid/liquid interface of FeP NAs/CC and FeP MPs/CC were measured to be 60 and 0.32 mF/cm^2, respectively (Figure S8), implying much higher surface roughness and surface area of FeP NAs/CC.[30] Both the better electrical connection between FeP NAs and CC and the higher surface area of FeP NAs/CC contribute to its superior catalytic activity.

We probed the durability for FeP NAs/CC by continuous cyclic voltammetric sweeps in 0.5 M H_2SO_4 solution +0.20 to −0.20 V vs RHE at a scan rate of 100 mV/s. The polarization curve shows a decay after the first 1000 cycles but retains stable catalytic activity after the 2000th and 5000th cycles (Figure 3).

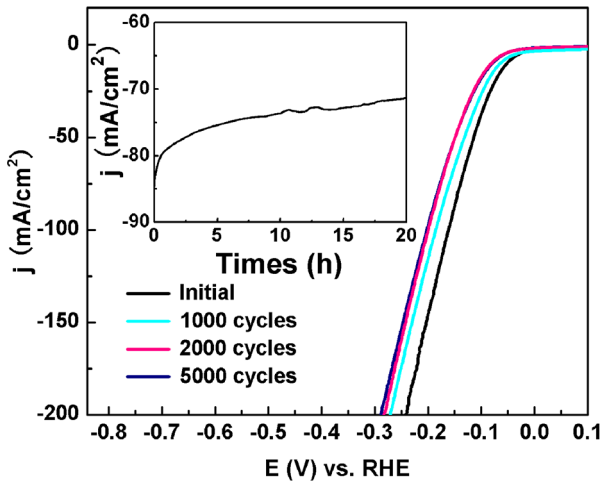

Figure 3. Stability of FeP NAs/CC with an initial polarization curve and after 1000, 2000, and 5000 cycles at a scan rate of 100 mV/s between +0.20 and −0.20 V in 0.5 M H_2SO_4 (inset: time-dependent catalytic current density curve during electrolysis for FeP NAs/CC in 0.5 M H_2SO_4 at η = 150 mV).

The durability of FeP NAs/CC was further tested by electrolysis at a fixed overpotential of 150 mV. The current density decreases from an initial value of 87 mA/cm^2 but remains at about 71 mA/cm^2 at the end of electrolysis for 20 h (Figure 3 inset). These observations suggest good electrochemical stability of this electrode. ICP-MS analysis of the electrolyte solution after stability test shows the presence of Fe. Such Fe species might come from corrosion or detachment of FeP from CC during electrolysis.[25] The Faradaic efficiency of this electrode for hydrogen evolution was determined to be close to 100% using a previously reported method,[28−31] as shown in Figure S9.

It should be pointed out that the FeP NAs/CC also performs well in both neutral and alkaline solutions. This electrode exhibits an onset overpotential of 112 mV and a Tafel slope of 71 mV/dec in 1 M phosphate buffer solution (PBS, pH = 7), as shown in Figure 4a. It shows onset overpotential of 86 mV and

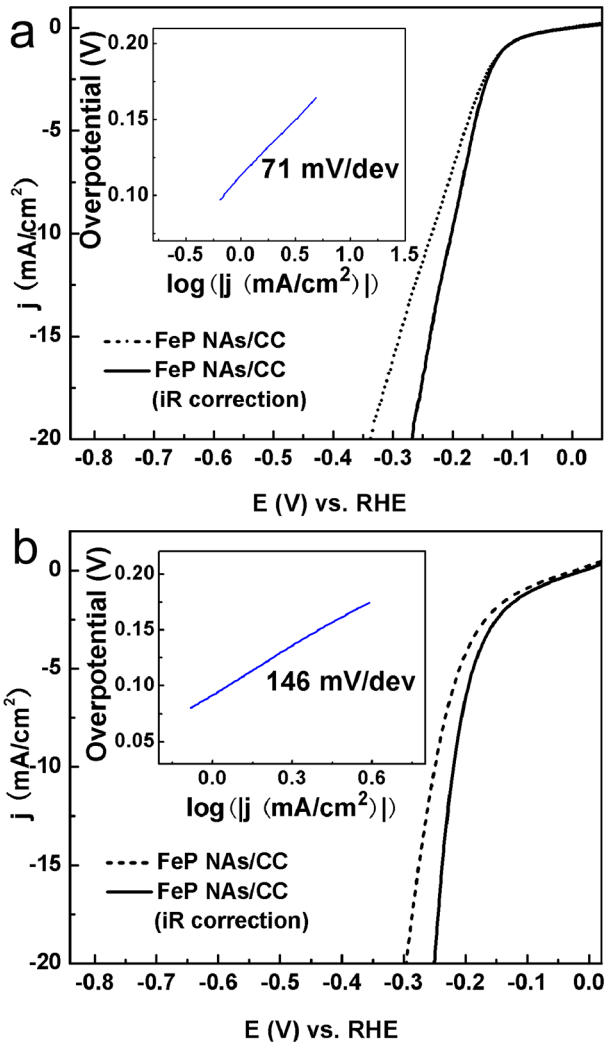

Figure 4. Polarization curve and Tafel slope for FeP NAs/CC in (a) 1 M PBS and (b) 1 M KOH.

a Tafel slope of 146 mV/dec in 1 M KOH (Figure 4b). Furthermore, to afford current density of 10 mA/cm^2, it only needs overpotentials of 202 and 218 mV in PBS and KOH, respectively. These overpotentials compare favorably to the behaviors of most reported non-noble-metal HER catalysts in neutral or alkaline media (Table S2 and S3).

Figure S10 shows the X-ray photoelectron spectroscopy (XPS) spectra in the Fe(2p) and P(2p) regions for FeP NAs/CC. The peaks for the binding energy (BE) of Fe $2p_{3/2}$ appear at 707.5 and 712 eV, whereas the peak for the BE of Fe $2p_{1/2}$ appears at 720.4 eV. The high-resolution P(2p) region shows two peaks at 130.3 and 129.7 eV, reflecting the BE of P $2p_{1/2}$ and P $2p_{3/2}$, respectively, along with one peak at 133.9 eV. The

dx.doi.org/10.1021/cs501106g | ACS Catal. 2014, 4, 4065−4069

peaks at 707.5 and 129.7 eV are close to the BE for Fe and P in FeP.[42] The peaks at 712 and 133.9 eV can be assigned to oxidized Fe and P species arising from superficial oxidation of FeP exposed to air.[43] The Fe 2p BE of 707.5 eV is positively shifted from that of metallic Fe (706.8 eV), although the P 2p BE of 129.7 eV shows negative shift from that of elemental P (130.2 eV).[44,45] It suggests that Fe and P in FeP carries a partial positive and negative charge (δ^-), respectively, due to the occurrence of electron transfer from Fe to P.[42,43,46] Metal complex HER catalysts incorporate proton relays from pendant acid−base groups positioned close to the metal center where hydrogen evolution occurs.[47,48] Like recently developed Ni_2P,[26] CoP,[28,29] Cu_3P,[30] and MoP[31] HER catalysts, FeP also features pendant base P (δ^-) positioned close to the metal center Fe (δ^+). It is believed that both Fe center and the pendant base P are the active sites for the hydrogen evolution. The Fe and P function as the hydride-acceptor and proton-acceptor center, respectively, facilitating the HER.[24,49] Note that this FeP catalyst shows similar numeric area of P(2p) region before (18530 CPS·eV) and after (17650 CPS·eV) electrolysis (Figure S11), implying the form of active catalyst is not changed by electrochemical experiments.

In conclusion, FeP nanorod arrays have been developed on carbon cloth for the first time through low-temperature phosphidation reaction. This FeP NAs/CC, as a binder-free 3D hydrogen evolution cathode, exhibits high catalytic activity and good stability in acidic media. It is also highly active in both neutral and alkaline solutions. Future work will focus on improving its long-term electrochemical stability to meet practical requirements in industrial and commercial operations.

■ ASSOCIATED CONTENT

Supporting Information

Experimental details; XRD patterns; EDX and XPS spectra; SEM images; Tables S1−S3; polarization curves; Nyquist plots; cyclic voltammetry; exchange current density calculation; Faradaic efficiency determination. This material is available free of charge via the Internet at http://pubs.acs.org.

■ AUTHOR INFORMATION

Corresponding Authors

*E-mail: sunxp@cwnu.edu.cn (X.S.).
*E-mail: luoylcwnu@hotmail.com (Y.L.).

Notes

The authors declare no competing financial interest.

■ REFERENCES

(1) Bard, A. J.; Fox, M. A. *Acc. Chem. Res.* **1995**, *28*, 141−145.
(2) Chow, J.; Kopp, R. J.; Portney, P. R. *Science* **2003**, *302*, 1528−1531.
(3) Dresselhaus, M. S.; Thomas, I. L. *Nature* **2001**, *414*, 332−337.
(4) Turner, J. A. *Science* **2004**, *305*, 972−974.
(5) Gray, H. B. *Nat. Chem.* **2009**, *1*, 7−7.
(6) Walter, M. G.; Warren, E. L.; McKone, J. R.; Boettcher, S. W.; Mi, Q.; Santori, E. A.; Lewis, N. S. *Chem. Rev.* **2010**, *110*, 6446−6473.
(7) Greeley, J.; Norskov, J. K.; Kibler, L. A.; El-Aziz, A. M.; Kolb, D. M. *ChemPhysChem* **2006**, *7*, 1032−1035.
(8) Sheng, W. C.; Gasteiger, H. A.; Shao-Horn, Y. *J. Electrochem. Soc.* **2010**, *157*, B1529−b1536.
(9) Le, G. A.; Artero, V.; Jousselme, B.; Tran, P. D.; Guillet, N.; Métayé, R.; Fihri, A.; Palacin, S.; Fontecave, M. *Science* **2009**, *326*, 1384−1387.
(10) Brown, D. E.; Mahmood, M. N.; Man, M. C. M.; Turner, A. K. *Electrochim. Acta* **1984**, *29*, 1551−1556.
(11) Raj, I. A.; Vasu, K. I. *J. Appl. Electrochem.* **1990**, *20*, 32−38.
(12) Jaramillo, T. F.; Jørgensen, K. P.; Bonde, J.; Nielsen, J. H.; Horch, S.; Chorkendorff, I. *Science* **2007**, *317*, 100−102.
(13) Kibsgaard, J.; Chen, Z.; Reinecke, B. N.; Jaramillo, T. F. *Nat. Mater.* **2012**, *11*, 963−969.
(14) Lukowski, M. A.; Daniel, A. S.; Meng, F.; Forticaux, A.; Li, L.; Jin, S. *J. Am. Chem. Soc.* **2013**, *135*, 10274−10277.
(15) Xie, J.; Zhang, H.; Li, S.; Wang, R.; Sun, X.; Zhou, M.; Zhou, J.; Lou, X.; Xie, Y. *Adv. Mater.* **2013**, *25*, 5807−5813.
(16) Kong, D.; Wang, H.; Cha, J. J.; Pasta, M.; Koski, K. J.; Yao, J.; Cui, Y. *Nano Lett.* **2013**, *13*, 1341−1347.
(17) Vrubel, H.; Hu, X. *Angew. Chem., Int. Ed.* **2012**, *54*, 12703−12706.
(18) Chen, W.; Wang, C.; Sasaki, K.; Marinkovic, N.; Xu, W.; Muckerman, J. T.; Zhu, R.; Adzic, R. R. *Energy Environ. Sci.* **2013**, *6*, 943−951.
(19) Cui, W.; Cheng, N.; Liu, Q.; Ge, C.; Asiri, A. M.; Sun, X. *ACS Catal.* **2014**, *4*, 2658−2661.
(20) Chen, W.; Sasaki, K.; Ma, C.; Frenkel, A. I.; Marinkovic, N.; Muckerman, J. T.; Zhu, R.; Adzic, R. R. *Angew. Chem., Int. Ed.* **2012**, *51*, 6131−6135.
(21) Cao, B.; Veith, G. M.; Neuefeind, J. C.; Adzic, R. R.; Khalifah, P. G. *J. Am. Chem. Soc.* **2013**, *135*, 19186−19192.
(22) Oyama, S. T.; Gott, T.; Zhao, H.; Lee, Y. K. *Catal. Today* **2009**, *143*, 94−107.
(23) Carenco, S.; Portehault, D.; Boissière, C.; Mèzailles, N.; Sanchez, C. *Chem. Rev.* **2013**, *113*, 7981−8065.
(24) Popczun, E. J.; McKone, J. R.; Read, C. G.; Biacchi, A. J.; Wiltrout, A. M.; Lewis, N. S.; Schaak, R. E. *J. Am. Chem. Soc.* **2013**, *135*, 9267−9270.
(25) Feng, L.; Vrubel, H.; Bensimon, M.; Hu, X. *Phys. Chem. Chem. Phys.* **2014**, *16*, 5917−5921.
(26) Pu, Z.; Liu, Q.; Tang, C.; Asiri, A. M.; Sun, X. *Nanoscale* **2014**, *6*, 11031−11034.
(27) Popczun, E. J.; Read, C. G.; Roske, C. W.; Lewis, N. S.; Schaak, R. E. *Angew. Chem., Int. Ed.* **2014**, *53*, 5427−5430.
(28) Liu, Q.; Tian, J.; Cui, W.; Cheng, N.; Asiri, A. M.; Sun, X. *Angew. Chem., Int. Ed.* **2014**, *53*, 6710−6714.
(29) Tian, J.; Liu, Q.; Asiri, A. M.; Sun, X. *J. Am. Chem. Soc.* **2014**, *136*, 7587−7590.
(30) Tian, J.; Liu, Q.; Cheng, N.; Asiri, A. M.; Sun, X. *Angew. Chem., Int. Ed.* **2014**, *53*, 9577−9581.
(31) Xing, Z.; Liu, Q.; Asiri, A. M.; Sun, X. *Adv. Mater.* **2014**, *26*, 5702−5707.
(32) Xiao, P.; Sk, M. A.; Thia, L.; Ge, X.; Lim, R. J.; Wang, J.; Lim, K. H.; Wang, X. *Energy Environ. Sci.* **2014**, *7*, 2624−2629.
(33) McEnaney, J. M.; Crompton, J. C.; Callejas, J. F.; Popczun, E. J.; Biacchi, A. J.; Lewis, N. S.; Schaak, R. E. *Chem. Mater.* **2014**, *26*, 4826−4831.
(34) McEnaney, J. M.; Crompton, J. C.; Callejas, J. F.; Popczun, E. J.; Read, C. G.; Lewis, N. S.; Schaak, R. E. *Chem. Commun.* **2014**, *50*, 11026−11028.
(35) Xu, R.; Wu, R.; Zhang, J.; Shi, Y.; Zhang, B. *Chem. Commun.* **2013**, *49*, 6656−6658.
(36) Luo, Y.; Jiang, J.; Zhou, W.; Yang, H.; Luo, J.; Qi, X.; Zhang, H.; Yu, D. Y. W.; Li, C. M.; Yu, T. *J. Mater. Chem.* **2012**, *22*, 8634−8640.
(37) Roy-Mayhew, J. D.; Boschloo, G.; Hagfeldt, A.; Aksay, I. A. *ACS Appl. Mater. Interfaces* **2012**, *4*, 2794−2800.
(38) Jiang, P.; Liu, Q.; Liang, Y.; Tian, J.; Asiri, A. M.; Sun, X. *Angew. Chem., Int. Ed.* DOI: 10.1002/anie.201406848.
(39) Liu, R.; Gu, S.; Du, H.; Li, C. M. *J. Mater. Chem. A* **2014**, *2*, 17263−17267.
(40) Pentland, N.; Bockris, J. O. M.; Sheldon, E. *J. Electrochem. Soc.* **1957**, *104*, 182−194.
(41) Conway, B. E.; Tilak, B. V. *Electrochim. Acta* **2002**, *47*, 3571−3594.
(42) Grosvenor, A. P.; Wik, S. D.; Cavell, R. G.; Mar, A. *Inorg. Chem.* **2005**, *44*, 8988−8998.

(43) Li, L.; Chen, C.; Chen, L.; Zhu, Z.; Hu, J. *Environ. Sci. Technol.* **2014**, *48*, 3372−3377.
(44) Rajesh, B.; Sasirekha, N.; Lee, S.; Kuo, H.; Chen, Y. *J. Mol. Catal. A: Chem.* **2008**, *289*, 69−75.
(45) *Practical Surface Analysis by Auger and X-ray Photoelectron Spectroscopy*; Briggs, D., Seah, M. P., Eds.; John Wiley & Sons: New York, 1983.
(46) *Encyclopedia of Inorganic Chemistry*, 2nd ed.; King, R. B., Ed.; John Wiley & Sons: Hoboken, NJ, 2005.
(47) Wilson, A. D.; Newell, R. H.; McNevin, M. J.; Muckerman, J. T.; Dubois, M. R.; Dubois, D. L. *J. Am. Chem. Soc.* **2006**, *128*, 358−366.
(48) Wilson, A. D.; Shoemaker, R. K.; Miedaner, A.; Muckerman, J. T.; Dubois, D. L.; Dubois, M. R. *Proc. Natl. Acad. Sci. U.S.A.* **2007**, *104*, 6951−6956.
(49) Liu, P.; Rodriguez, J. A. *J. Am. Chem. Soc.* **2005**, *127*, 14871−14878.